Food Chemistry 424 (2023) 136441

Contents lists available at ScienceDirect

Food Chemistry

journal homepage: www.elsevier.com/locate/foodchem

Spatio-temporal distribution patterns and quantitative detection of aflatoxin B_1 and total aflatoxin in peanut kernels explored by short-wave infrared hyperspectral imaging

Zhen Guo[a,b,c], Jing Zhang[a], Haowei Dong[a,b,c], Jiashuai Sun[a,b,c], Jingcheng Huang[a,b,c], Shiling Li[a,b,c], Chengye Ma[a], Yemin Guo[a,b,c,*], Xia Sun[a,b,c,*]

[a] School of Agricultural Engineering and Food Science, Shandong University of Technology, No. 266 Xincun Xilu, Zibo, Shandong 255049, China
[b] Shandong Provincial Engineering Research Center of Vegetable Safety and Quality Traceability, No. 266 Xincun Xilu, Zibo, Shandong 255049, China
[c] Zibo City Key Laboratory of Agricultural Product Safety Traceability, No. 266 Xincun Xilu, Zibo, Shandong 255049, China

ARTICLE INFO

Keywords:
Short-wave infrared
Hyperspectral imaging
Aspergillus flavus
Aflatoxin
Peanut kernels

ABSTRACT

Aflatoxin contamination in peanut kernels seriously harms the health of humans and causes significant economic losses. Rapid and accurate detection of aflatoxin is necessary to minimize its contamination. However, current detection methods are time-consuming, expensive and destructive to samples. Therefore, short-wave infrared (SWIR) hyperspectral imaging coupled with multivariate statistical analysis was used to investigate the spatio-temporal distribution patterns of aflatoxin, and quantitatively detect the aflatoxin B_1 (AFB_1) and total aflatoxin in peanut kernels. In addition, *Aspergillus flavus* contamination was identified to prevent the production of aflatoxin. The result of validation set demonstrated that SWIR hyperspectral imaging could predict the contents of the AFB_1 and total aflatoxin accurately, with residual prediction deviation values of 2.7959 and 2.7274, and limits of detection of 29.3722 and 45.7429 μg/kg, respectively. This study presents a novel method for the quantitative detection of aflatoxin and offers an early warning system for its potential application.

1. Introduction

Peanut kernels are rich sources of protein, fat, vitamins and dietary fiber, and can be consumed directly or processed into peanut butter and edible oil (Higgs, 2003). However, during storage and transportation, peanut kernels are vulnerable to contamination by toxigenic fungi, particularly *Aspergillus flavus* and *Aspergillus parasiticus*. These fungi produce aflatoxins, which are highly toxic and carcinogenic secondary metabolites (Liu et al., 2011). Aflatoxins are furanocoumarin derivatives that are divided into four subgroups including aflatoxin B_1 (AFB_1), aflatoxin B_2 (AFB_2), aflatoxin G_1 (AFG_1), and aflatoxin G_2 (AFG_2) (Wu, Xie, & Xu, 2018). Among these subgroups, AFB_1 is the most toxic, which is commonly present in peanut kernels and corn kernels (Qiao et al., 2017). The toxic effect of AFB_1 on the liver tissue of humans and animals can lead to liver cancer and even death (Gao et al., 2021). Although AFB_2, AFG_1 and AFG_2 are less toxic than AFB_1, they can also cause serious harm to humans, especially presenting in high concentrations. The contents of these subgroups of aflatoxins collectively increase the total amount of aflatoxin, which can have a greater impact on human health. To mitigate the risks posed by aflatoxin exposure, many countries have established safety limits for AFB_1 and total aflatoxin (the sum of AFB_1, AFB_2, AFG_1, and AFG_2) in food. The worldwide accepted range for AFB_1 and total aflatoxin is 0–20 μg/kg and 0–35 μg/kg, respectively (Food and Agriculture Organization (FAO) (FAO), 2004). In the European Union, the safety limits for AFB_1 and total aflatoxin are 2 μg/kg and 4 μg/kg, respectively, which peanut kernels are intended for human consumption (Ghali et al., 2009). In Japan, the safety limit for AFB_1 is 10 μg/kg in all foods (Ding, Li, Bai, & Zhou, 2012). In China, the safety limit for AFB_1 is 20 μg/kg in peanuts and their products since 2017. The impact of aflatoxin toxicity and strict regulations on international peanut kernel trade is significant, with 89% of alerts attributed to aflatoxins in the EU Rapid Alert System for Food and Feed triggered between 2010 and 2019 (Krska et al., 2022). While the detection of AFB_1 has been widely studied, few reports on the quantitative detection of total aflatoxin using hyperspectral imaging are available.

Currently, wet-chemical methods, such as liquid chromatography coupled to tandem mass spectrometry (LC-MS/MS) and high-performance liquid chromatography with fluorescence detection

* Corresponding authors at: School of Agricultural Engineering and Food Science, Shandong University of Technology, No. 266 Xincun Xilu, Zibo, Shandong 255049, China.

https://doi.org/10.1016/j.foodchem.2023.136441
Received 14 December 2022; Received in revised form 17 May 2023; Accepted 19 May 2023
Available online 20 May 2023
0308-8146/

(HPLC-FLD), are commonly used to detect aflatoxins (Freitag et al., 2022). These methods have the advantage of high accuracy and allow low detection limits. However, they are time-consuming, expensive and damaging to samples. To address these limitations, hyperspectral imaging technology has been introduced, which can detect the external and internal quality of food and agricultural products rapidly and non-destructively. It has been extensively used to identify fungal contamination in peanut kernels and maize kernels, as well as detect aflatoxin contamination in almonds (Liu et al., 2020; Tao et al., 2021; Mishra et al., 2022). Meanwhile, the application of hyperspectral imaging to detect fungal contamination has been recently summarized (Freitag et al., 2022). Short-wave infrared (SWIR) hyperspectral imaging provides information on vibrations of overtones and combination bands in the regions of 1,000 to 2,500 nm, such as O—H (water, carbohydrates), N—H (proteins), and C—H (lipids) (Kimuli et al., 2018). Therefore, SWIR hyperspectral imaging technology coupled with multivariate statistical analysis could detect hydrogen-containing organic compounds such as aflatoxin by analyzing the functional group information in specific spectra bands.

In addition, the physical structure and chemical composition of peanut kernels undergo significant changes when the kernels are contaminated by *Aspergillus flavus*. Firstly, the coat of peanut kernel will be contaminated by *Aspergillus flavus*, causing it to break and grow mycelia. Then, the spores of *Aspergillus flavus* directly enter the cotyledons through the broken seed coat, and the mycelium penetrates the embryonic tissue and builds up between and within cells, causing the overall distortion of the intercellular tissue (Achar et al., 2009). During this process, total sugars, fats, proteins and other substances are decomposed and utilized for the constant proliferation and metabolism of *Aspergillus flavus*, producing secondary metabolites such as aflatoxin continuously (Sharma et al., 2021). Although SWIR hyperspectral imaging may not have the direct sensitivity to detect aflatoxin, it is possible to detect for aflatoxin by measuring changes in the sample induced by fungi (Freitag et al., 2022). However, the relationship among the spectral information, the structure and composition of peanut kernels has not been revealed, and the spatio-temporal distribution patterns of aflatoxin during the process of *Aspergillus flavus* contamination have not been visually studied using hyperspectral imaging. It is particularly essential to explore these distribution patterns and to quantitatively detect the content of aflatoxin in peanut kernels, reducing agricultural products loss and avoiding harm to human health. Moreover, precise and rapid identification of contaminated peanut kernels is necessary to prevent aflatoxin from entering a food chain. While there are already several researches of kernel sorting to reduce aflatoxin content of a bulk corn samples either relying on single-kernel near infrared spectroscopy (SKNIR) or hyperspectral imaging but not yet for aflatoxins in peanut kernels (Freitag et al., 2022).

Therefore, the objectives of this study are (1) to analysis the spatio-temporal distribution patterns of aflatoxin and spectral information changes in peanut kernels, (2) to identify the contamination of *Aspergillus flavus* in peanut kernels and determine the contamination time, (3) to classify aflatoxins in contaminated peanut kernels using safety limits as a threshold, and (4) to evaluate a feasibility of using SWIR hyperspectral imaging to quantitatively detect the contents of AFB_1 and total aflatoxin.

2. Materials and methods

2.1. Sample preparation and aflatoxin detection

Peanut kernels were purchased from a market in Zibo City, Shandong Province, and the variety of peanut kernels was "Weihua". A total of 1260 clean peanut kernels with similar sizes, no defects and no germination were selected manually, and the average weight of a single peanut kernel was 1.022 ± 0.100 g. The kernels were sterilized by soaking in 75% ethanol solution for 1 min, rinsed 3 times with sterile water, and dried in a sterile environment. The contaminated group included 840 peanut kernels, while the control group consisted of the remaining 420 peanut kernels.

The toxigenic strain of *Aspergillus flavus* (ATCC#28539) was obtained from the National Strain Center of China and was inoculated on high-temperature sterilized PDA medium, then incubated at 28 °C for 5 d under dark conditions. The conidia were collected and diluted to a concentration of 1×10^6 CFU/mL with sterile water. Peanut kernels inoculated with the spore suspension were used as the contaminated groups and those inoculated with sterile water were used as the control groups. 18 groups were set up, including 12 contaminated groups and 6 control groups, with each group containing 70 peanut kernels. Hyperspectral images were taken from 14 peanut kernels from each group every 2 d from the 1st day to the 9th day after inoculation. Then, a single peanut kernel was randomly selected from every 7 peanut kernels to detect the content of aflatoxin by HPLC-FLD, as it was not feasible to determine the aflatoxin content of all 1260 peanut kernels. The incubator was set to 30 °C and 85% relative humidity to simulate the mildewing process of peanut kernels in a natural environment (Long, Huang, Wang, Fan, & Tian, 2022).

After hyperspectral images being acquired, the contents of AFB_1, AFB_2, AFG_1 and AFG_2 in peanut kernels were measured using a HPLC-FLD system (1260 Infinity II LC System, Agilent Technologies, Santa Clara, CA) with an analytical column (4.6 mm × 150 mm with 4 μm particle size; Poroshell 120, Agilent Technologies, Santa Clara, CA). The HPLC-FLD separation and quantitative analysis was achieved using a mobile phase consisting of acetonitrile: methanol: water (16:16:68, *v/v/v*) at a flow rate of 1.0 mL/min and a temperature of 40 °C. The aflatoxins were detected and quantified with fluorescence detection at 360 nm (excitation) and 440 nm (emission) wavelengths, following the method described by Campos, Rosas, Neto, Mello, and Vasconcelos (2017).

2.2. Hyperspectral image acquisition and calibration

A SWIR scanning hyperspectral imaging system (900–2,500 nm) (HSI-eSWIR-1000-2500, Isuzu Optics Corp, Taiwan, China) was used to obtain hyperspectral images. All components were installed in a dark box to avoid the influence of ambient light.

Each hyperspectral image contained 28 peanut kernels, and a total of 36 hyperspectral images were obtained. The speed of the mobile platform was set to 15.34 mm/s and the exposure time was set to 2.9 ms during the process of acquiring hyperspectral images. The original images were calibrated using a black reference image and a white reference image to eliminate the effects of ambient noise and dark current. The relevant correction formula was described by Sun et al. (2019). To eliminate the instrument error, a spectral in the range of 963–2,200 nm was retained.

The OTSU method (OTSU) was used to automatically generate the best segmentation threshold according to the image (Huang, Li, & Wen, 2021). This adaptive threshold judgment method was used to select the region of interest (ROI) of every single peanut kernel from the hyperspectral images. Fig. S1 showed the process of hyperspectral image segmentation. Firstly, a gray image with the largest difference in reflectance between the background and peanut kernels was selected from the raw hyperspectral image. Then, OTSU was used to segment the gray image and generate a mask image, which the background and peanut kernels were represented by 0 and 1 pixel, respectively. And then, the mask was multiplied by each band image in the raw hyperspectral image to generate a mask hyperspectral image with only peanut kernels. Finally, the ROI of each single peanut kernel was selected, and average spectra of the ROI were used as the spectra of the single peanut kernel.

2.3. Multivariate statistical analysis

2.3.1. Discriminant analysis

In this study, principal component analysis (PCA) was utilized as a data compression method for dimensionality reduction and preliminary characterization of raw spectral data (Tao et al., 2021). Furthermore, 5 discriminant analysis models were applied in this study including linear discriminant analysis (LDA), principal component analysis-linear discriminant analysis (PCA-LDA), partial least squares-discriminant analysis (PLS-DA), soft independent modeling of class analogy (SIMCA) and *k*-nearest neighbors (K-NN). A sample set partitioning based on joint x–y distance (SPXY) was used to divide the sample set into a calibration set and a validation set according to the quantity ratio of 3:1 (Wang et al., 2021; Sun et al., 2021). The effectiveness of each model was evaluated using the accuracy rate, and the false-negative rate of the contaminated-control group was calculated using a formula described by Wu et al., (2020).

2.3.2. Regression analysis

Partial least squares regression (PLSR) and principal component regression (PCR) were used for aflatoxin regression analysis. PLSR was a linear regression model, which could effectively solve the problem of high linear correlation of hyperspectral data by indirectly describing the relationship between dependent variables and independent variables (Wold, Sjöström, & Eriksson, 2001). PCR also was a linear regression model, it could fully utilize all spectral data and iteratively perform factor analysis (Yin et al., 2012). Hyperspectral images contained hundreds of wavelengths with a lot of redundant and useless information. Therefore, the successive projection algorithm (SPA), regression coefficient (RC), competitive adaptive reweighted sampling (CARS), interval variable iterative space shrinkage approach (IVISSA), and the interval variable iterative space shrinkage approach combined with the successive projection algorithm (IVISSA-SPA) were used to select feature wavelengths to eliminate redundant data. SPXY was also used to divide the sample set with a quantity proportion of 3:1.

The coefficients of correlation (R^2) of calibration (R^2_C), cross-validation (R^2_{CV}) and validation (R^2_V) were calculated to evaluate the performance of the model. Meanwhile, root mean square errors (RMSE) of calibration (RMSEC), cross-validation (RMSECV), validation (RMSEV) and residual prediction deviation (RPD) were calculated to evaluate the effectiveness of the model. Generally, a model with a higher R^2, RPD and lower RMSE had a better effect. In addition, the limit of detection (LOD) and the limit of quantification (LOQ) were calculated to evaluate the detection limits of the model (Adedipe, Johanningsmeier, den Truong, & Yencho, 2016). The Unscrambler X 10.4 (CAMO Software, Oslo, Norway) and MATLAB R2016a (MathWorks, Natick, USA) were used for multivariate analysis.

3. Results and discussion

3.1. Statistical analysis of aflatoxin accumulation over time in peanut kernels

Aflatoxins were found in all contaminated groups, while the control groups had no aflatoxins according to HPLC-FLD results. Furthermore, the contaminated groups had 66 samples exceeding the safety limit for total aflatoxin (35 μg/kg) and 74 samples exceeding the safety limit for AFB_1 (20 μg/kg). Table S1 showed that the order of the content of various aflatoxins in peanut kernels from high to low, which was AFB_1, AFB_2, AFG_2, and AFG_1, and almost no AFG_1 was produced. The LOD, LOQ and relative standard deviation (RSD) of the HPLC-LFD reference method had been provided in Table S2. AFB_1 was the major aflatoxin produced by *Aspergillus flavus* in peanut kernels, which had been confirmed in another study (Mphande, Siame, & Taylor, 2004). Roasted peanut kernels from Nigeria had an average content of 25.5 ppb AFB_1 and 10.7 ppb AFB_2, which was close to the content obtained in this work (Bankole, Ogunsanwo, & Eseigbe, 2005). Fig. 1 showed that aflatoxin in peanut kernels accumulated higher over time. The result showed that aflatoxin content was low on the 1st day after inoculation, which might correspond to initial *Aspergillus flavus* spore germination, fungal penetration into peanut tissues, and mycelia growth during this period. Later, *Aspergillus flavus* began reproductive growth and started secondary metabolism on the seed coat in 36–48 h. Therefore, the aflatoxin content increased on the 3rd day compared with the 1st day. Then, aflatoxins continued to accumulate in peanut kernels, reaching a higher level on the 5th day and maintaining a steady increase, which might correspond to *Aspergillus flavus* spores entering peanut cotyledon through the cracked seed coat and beginning proliferation after 72 h (Achar et al., 2009). Finally, the maximum aflatoxin content was reached on the 9th day. It was worth noting that the average content of AFB_1 and total aflatoxin in the contaminated groups exceeded the safety limits (20 μg/kg and 35 μg/kg, respectively) on the 5th day after the inoculation.

3.2. Spectra analysis

Fig. 2 showed the average original spectra and average Savitzky-Golay smoothing-second derivative (SG-2nd derivative) preprocessed spectra of peanut kernels. A total of 1260 spectral curves were used in this work, with the control groups containing 420 spectral curves and each contaminated group containing 168 spectral curves. Firstly, Fig. 2 (a) illustrated that the spectral reflectance curves of the control groups and 5 contaminated groups exhibited a similar trend of change. Secondly, Fig. 2(b) showed that the spectral reflectance of the contaminated groups was lower than that of the control groups in the range of 1,000–2,036 nm except 1,861 nm. Furthermore, the original spectra showed main reflectance peaks at 1,114, 1,302 and 1,861 nm in Fig. 2(a) and Fig. 2(b). The 1,114 nm was associated with the second overtone C—H stretching and the 1,302 nm corresponded to the combined C—H stretching (Stuart, 2004). The 1,861 nm was related to the combination of C—O and O—H stretching (Kimuli et al., 2018; Berardo et al., 2005). Finally, minor spectral differences between control and contaminated peanut kernels were amplified by performing the SG-2nd derivative

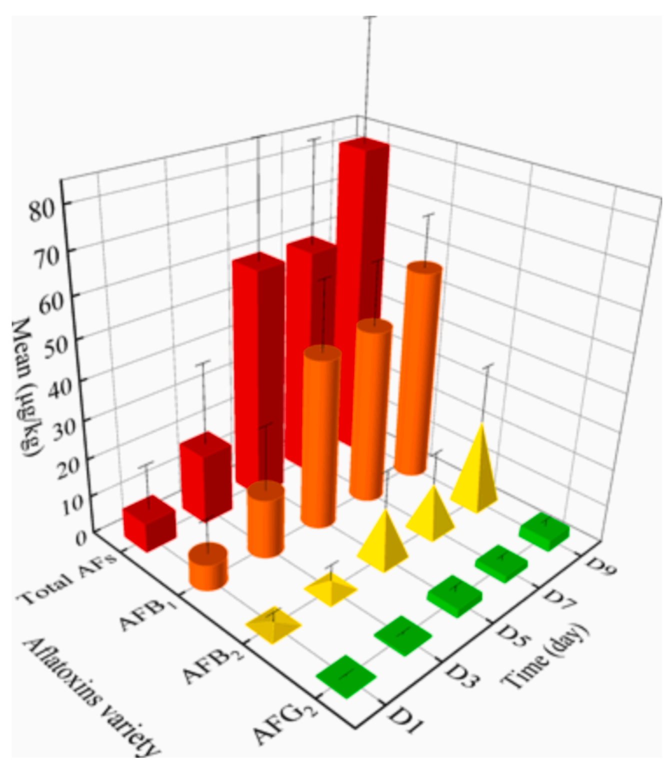

Fig. 1. Aflatoxin contents in peanut kernel for different storage time.

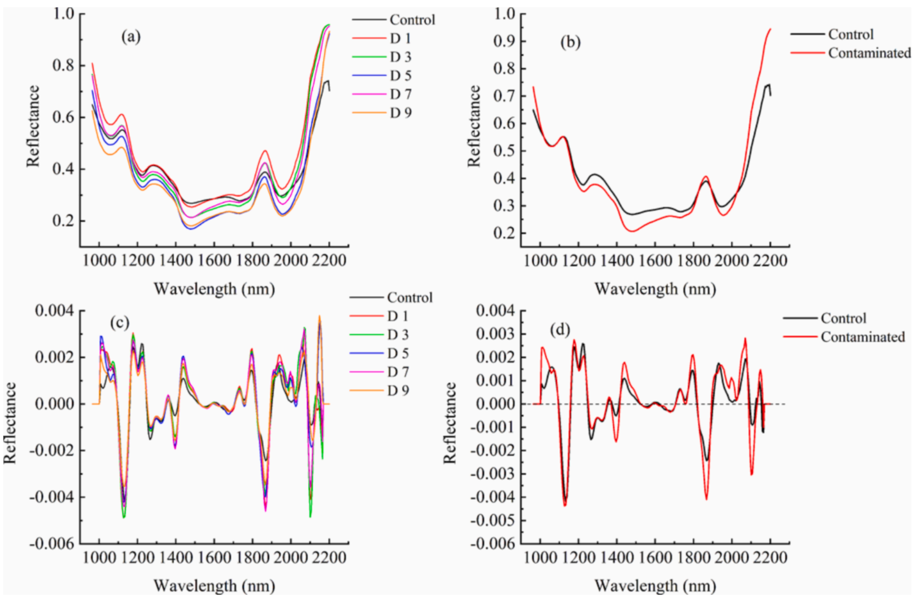

Fig. 2. Average original spectra and average Savitzky-Golay smoothing-second derivative (SG-2nd derivative) preprocessed spectra of peanut kernels, (a) average original spectra of the control group and 5 contaminated groups, (b) average original spectra of the control group and contaminated group, (c) average SG-2nd derivative preprocessed spectra of the control group and 5 contaminated groups, (d) average SG-2nd derivative preprocessed spectra of the control group and the contaminated group.

pretreatment at 1,221, 1,265, 1,302, 1,396, 1,440, 1,797, 1,867, 1,964 and 2,068 nm in Fig. 2(c) and (d). All these spectral differences indicated that physical and chemical changes were caused by fungal contamination in the *Aspergillus flavus*-peanut kernels interaction. Moreover, fungal metabolic activity was inevitably a dominant factor affecting the spectral changes after reaching a certain contamination level (Kaya-Celiker, Mallikarjunan, & Kaaya, 2015).

3.3. Identification of Aspergillus flavus contamination

3.3.1. Pca

PCA was performed on the raw spectral data of peanut kernels in the contaminated groups and the control groups to achieve a preliminary characterization of spectral data. Fig S2 showed that the first 6 principal components (PC 1 to PC 6) explained 99.93% of the model variance, with PC 1 contributing 97.94%, followed by PC 2, PC 3, PC 4, PC 5, and PC 6 contributing 0.84%, 0.74%, 0.22%, 0.15%, and 0.05% of the variance, respectively. Fig. S3 showed the distribution of different groups of raw spectral data in the 2-dimensional principal component space. The separation trend between the 5 contaminated groups and the control groups could not be observed in Fig. S3(a). It could be clearly distinguished in Fig. S3(b), but there was no obvious separation between the 5 contaminated groups. The reason might be due to the invalidity of the unsupervised PCA method. This method provided some important information about the basic data structure, which was used to visualize the dimensional space, but it was not considered an effective statistical test between groups (Kimuli et al., 2018). Therefore, the supervised discrimination method was needed to further analyze the spectral data of peanut kernels.

3.3.2. Classification of Aspergillus flavus contamination

Table 1 showed the classification effects of 5 discriminant models for different groups of contaminated peanut kernels and control peanut kernels. The control-contaminated group and the control-different contamination time groups (control-day 1 group, control-day 3 group, control-day 5 group, control-day 7 group and control-day 9 group) were classified into 2 categories, while the control-day 1-day 3-day 5-day 7-day 9 group was classified into 6 categories, and a false negative rate of the control-contaminated group was calculated. Firstly, in the classification of 2 categories, the calibration set and validation set of all models achieved an accuracy rate of >95.92%, and the false negative rate of <1.41%, indicating that accurate classification of healthy samples and contaminated samples. Secondly, for the classification of the control-day 1-day 3-day 5-day 7-day 9 group, SIMCA was used for the classification of 5 categories at most, so its results were not counted. And the average accuracy rates of the calibration set and validation set were 85.66% and 87.94% for the LDA, PCA-LDA, PLS-DA and K-NN models, demonstrating that the discriminant models could also distinguish the contamination time of peanut kernels. In addition, among the 5 models, LDA had the best classification effect, with the average classification accuracy rates reaching 100% and 99.53% in the calibration set and validation set, and the false negative rate being 0, indicating its ideal classification of different groups. Fig. S4 showed the classification effect of LDA in the control-day 1-day 3-day 5-day 7-day 9 group and the control-contaminated group, the dashed line showed the calibration set data to the left and the validation set data to the right. All the results demonstrated that the supervised discriminant model could accurately classify *Aspergillus flavus* contamination, and the difference in the spectra between the control groups and the contaminated groups was due to chemical and physical property changes caused by *Aspergillus flavus* during the peanut kernel contamination process.

The detection of *aspergillus* contamination levels in peanuts using electronic nose and near-infrared spectroscopy was investigated in a study aimed at identifying contamination of fungi in peanut kernels (Shen et al., 2018). Shen's study reported a classification accuracy rate of 92.11% and a false negative rate of 4.41% based on LDA using near-infrared spectroscopy, and stored contaminated peanut kernels for 9 d, as was done in this study. SWIR hyperspectral imaging was used to identify the prepared contaminated peanut kernels, reporting accuracy rates of >94% for the learning image and validation image (Qiao et al., 2017). Qiao's study also investigated the selection of hyperspectral image features from naturally moldy peanut kernels. Key wavelength bands and an ensemble classifier were used to identify the moldy peanuts, which achieved the classification accuracy rates of 95.31% and 97.36% based on PLS-DA and SIMCA, respectively (Yuan, Jiang, Qi, Xie, & Zhang, 2020). The result of this work was close to that of Yuan's study. Near-infrared hyperspectral imaging was used to identify the moldy kernels, with accuracy rates of 87.14% and 98.73% in learning image and validation image, respectively (Jiang, Qiao, & He, 2016).

3.4. Classification of aflatoxins in contaminated peanut kernels

The contaminated groups were classified using safety limits as thresholds to identify AFB_1 (20 μg/kg) and total aflatoxin (35 μg/kg),

Table 1
Classification effects of 5 different discriminant models of contaminated peanut kernels.

Group	Sample set		LDA		PCA-LDA		PLS-DA		SIMCA		K-NN	
	Calibration	Validation	Calibration	Validation	Calibration	Validation	Calibration	Validation	Calibration	Validation	Calibration	Validation
Control-day 1	441	147	100.00	99.32	100.00	100.00	100.00	100.00	100.00	100.00	100.00	99.32
Control- day 3	441	147	100.00	100.00	100.00	100.00	100.00	100.00	100.00	98.64	100.00	99.32
Control- day 5	441	147	100.00	100.00	99.77	97.96	100.00	100.00	100.00	98.64	98.87	97.76
Control- day 7	441	147	100.00	100.00	100.00	100.00	100.00	100.00	100.00	98.64	99.77	99.32
Control- day 9	441	147	100.00	99.32	100.00	100.00	100.00	100.00	100.00	98.64	98.87	95.92
Control- day 1 - day 3 - day 5 - day 7 -day 9	945	315	100.00	98.10	82.10	81.59	84.13	83.17	—	—	76.40	88.89
Control-contaminated	945	315	100.00	100.00	99.79	100.00	99.89	100.00	99.89	99.05	99.47	99.37
False negative rate	945	315	0.00	0.00	0.00	0.00	0.00	0.00	0.16	1.41	0.48	0.94

Note: LDA, linear discriminant analysis; PCA-LDA, principal component analysis combined with linear discriminant analysis; PLS-DA, partial least squares-discriminant analysis; SIMCA, soft independent modeling of class analogy; K-NN, *k*-nearest neighbors; "—", without value.

and the results were shown in Table 2. As LDA required that the number of variables in the data was greater than that of samples, PCA-LDA, PLS-DA, SIMCA and K-NN were used to classify the AFB_1 and total aflatoxin. Firstly, SIMCA achieved the best classification effect for total aflatoxin, with accuracy rates of 95.60% and 79.31% for the calibration set and validation set, respectively. Meanwhile, for AFB_1, the best result was achieved by PLS-DA with accuracy rates of 94.51% and 89.66% for the calibration set and validation set, respectively. In general, the average classification accuracy rates of the calibration set and validation set of total aflatoxin were 87.09% and 72.42% respectively, and those of AFB_1 were 88.74% and 83.60% respectively. These results indicated that the supervised discriminant model could accurately classify total aflatoxin and AFB_1, and the average classification accuracy rate of AFB_1 is higher than that of total aflatoxin.

In the study of classifying aflatoxins in peanut kernels, discrimination of naturally AFB_1 contamination peanuts was investigated based on a threshold of 20 ppb, LDA achieved the classification with an accuracy rate of 90% and 92% for the calibration set and validation set, respectively (He et al., 2021). The classification accuracy rate achieved in this work was similar to that of He's study. In their study, the integration of spectral features and texture features improved the accuracy rates of SVM to 93% and 94% for the calibration set and validation set, respectively. SWIR hyperspectral imaging was used to detect AFB_1 in a single maize kernel, and the AFB_1 contamination levels were divided into three groups (<20 ppb, 20–100 ppb, ≥100 ppb), with 71, 24 and 25 samples in each group, respectively (Chu et al., 2017). The overall classification accuracy rates of the calibration set and validation set were 83.75% and 82.50%, respectively. The classification achieved good results for the low level of <20 ppb in the calibration set and validation set (95.56%, 96.15%), and general results for the high level of >100 ppb (82.35%, 75.00%).

3.5. Quantitative analysis of aflatoxin content

To explore the feasibility of the SWIR hyperspectral imaging technology for detecting aflatoxin content in peanut kernels, PLSR and PCR were used to conduct regression analysis based on full spectra and feature wavelengths. Table 3 presented the parameter values for the performance of all models.

3.5.1. Quantitative analysis of regression model based on full spectra

Firstly, the PLSR and PCR based on the full spectra had a general prediction effect on the content of AFB_1 and total aflatoxin ($R_V^2 >$ 0.8340, RMSEV < 13.5320, RPD > 2.4487), while the prediction effect on the content of AFB_2 was poor ($R_V^2 > 0.7150$, RMSEV < 5.1339, RPD > 1.9153), and the content of AFG_2 could not be effectively predicted (R_V^2 > 0.5675, RMSEV < 0.9859, RPD > 1.5548). Moreover, no significant difference was observed between the prediction effect of PLSR and PCR models based on the full spectra. The average R_V^2, RMSEV and RPD values of PLSR were 0.7432, 7.0239 and 2.1668, and those of PCR were 0.7503, 7.0853 and 2.1724, respectively. However, PLSR had a smaller optimal number of principal components than PCR, which was 11, 18, respectively. Fig. 3 showed the regression effect of PLSR in predicting aflatoxin content, Fig. 3(a) and (b) showed that samples of the validation set were evenly distributed on both sides of the regression line, and the distribution of sample was quite scattered in Fig. 3(c) and (d). In addition, more samples were concentrated near the Y-axis in Fig. 3(d), which might be attributed to the small reference values of AFG_2. Therefore, future work was needed to increase the sample sizes and expand the data volume. To realize rapid detection and analysis, variable selection methods were used to select feature wavelengths.

3.5.2. Quantitative analysis of regression model based on feature wavelengths

First, the number of wavelengths was reduced from 209 to an average of 13, 14, 19 and 76 after conducting SPA, RC, CARS and

Table 2
Result of the classification of aflatoxins.

Group	Sample set		PCA-LDA		PLS-DA		SIMCA		K-NN	
	Calibration	Validation	Calibration	Validation	Calibration	Validation	Calibration	Validation	Calibration	Validation
Total aflatoxin	91	29	84.62	72.41	95.6	79.31	90.11	75.89	78.02	62.07
AFB_1	91	29	90.11	89.66	93.41	75.86	94.51	89.66	76.92	79.31

Note: PCA-LDA, principal component analysis combined with linear discriminant analysis; PLS-DA, partial least squares-discriminant analysis; SIMCA, soft independent modeling of class analogy; K-NN, *k*-nearest neighbors.

IVISSA. However, IVISSA retained a large number of wavelengths, accounting for 36.4% of the full spectra. Therefore, SPA was used to achieve the second wavelength selection after the selection of the IVISSA, and the number of feature wavelengths was reduced to an average of 16 by IVISSA-SPA. The selected feature wavelengths reduced the redundancy of spectral information. Generally, regression models based on different variable selection methods had obvious differences. The effect of the regression model based on SPA, IVISSA and IVISSA-SPA was significantly better than that of RC and CARS. The average RPD values of them were 2.2290, 2.1678, 2.2475, 1.8049 and 2.0336, respectively. Secondly, the IVISSA-SPA-PLSR model had a good effect in predicting the content of the AFB_1 and total aflatoxin, while the CARS-PLSR model achieved the best prediction results for the content of AFB_2, and the SPA-PLSR model showed the best performance in predicting the content of AFG_2. In general, according to the analysis of parameter values such as R_V^2, RMSEV, LOD and LOQ, PLSR and PCR based on the full spectra and feature wavelengths accurately predict the content of AFB_1 and total aflatoxin, with minor difference in the prediction effect between them, mainly because AFB_1 accounted for a large proportion of the total amount of aflatoxin. General prediction could only be made for the AFB_2, and AFG_2 content could not be effectively predicted due to the lower content of AFB_2 and AFG_2, which failed to cause the response of spectra. And the distribution of the sample data was skewed, which was mostly concentrated between 0–30 μg/kg and 0–4 μg/kg. Further studies required a larger sample set with more balanced AFB_2 and AFG_2 content distributions.

SWIR hyperspectral imaging was used to quantitatively detect the content of AFB_1 in corn kernels (Lu et al., 2022). PLSR and SVM models achieved acceptable performance ($R_V^2 \geq 0.89$, $RMSE_V \leq 3.370$, and RPD ≥ 2.48). The RPD value indicated that the prediction effect of this work was comparable to that of Lu's study. The content of AFB_1 was also quantitatively detected in corn kernels using SWIR hyperspectral imaging (Chu et al., 2017). The prediction effect of ($R_V^2 = 0.8663$) in this work was slightly better than that of SVM ($R_C^2 = 0.77$, $R_V^2 = 0.70$) in Chu's study for predicting the content of AFB_1. SWIR hyperspectral imaging was applied to rapidly predict the content of AFB_1 in mononuclear almonds, and the R^2 and RMSEP values of the model were 0.948 and 0.090 μg/g, respectively (Mishra et al., 2022). The R_V^2 value of IVISSA-SPA-PLSR in this work was slightly lower than that of MLR in Mishra's study. A fluorescence spectroscopy system was used to detect AFB_1 contamination pistachios (Wu and Xu, 2020). And the LOD value of IVISSA-SPA-PLSR reached 29.3722 μg/kg in this work which was similar to that of CARS-PLS (27.54 μg/kg) in Wu's study, although the instruments used were different.

In general, the comparison with related studies confirmed that SWIR hyperspectral imaging technology could qualitatively and quantitatively detect AFB_1 in peanut kernels. In addition, this study innovatively demonstrated the feasibility of detecting the content of total aflatoxin.

3.5.3. Discussion on the biological significance of feature wavelengths

The frequency of all selected feature wavelengths by the 5 algorithms were calculated, and the biological significance of these wavelengths were discussed. Fig. S5 showed that there were 5 distinct high-frequency wavelength peaks around 1,089, 1,358, 1,612, 1,732, and 2,122 nm, respectively. The first 19 high-frequency wavelengths included 2,122, 1,612, 1,089, 1,618, 1,732, 1,358, 2,095, 2,169, 1,605, 1,624, 1,352, 1,346, 963, 1,063, 1,340, 1,120, 1,630, 1,057, and 2,041 nm, respectively. Among these, wavelengths including 963, 1,057, 1,063, 1,089, and 1,120 nm were found to be closely associated with the fungal contamination, as they were linked to the free radical structure in the cell wall and N—H bond in most amino acids and aromatic rings. These changes in substance composition and cell structure of peanut kernel cells were likely associated with contamination by *Aspergillus flavus* (Fernández-Ibañez et al., 2009). Additionally, the high-frequency wavelength peak at 1,120 nm was close to 1,114 nm, which might be related to the stretching of the second overtone C—H, while the high-frequency wavelength peak at 1,732 nm was related to the first overtone of the C—H structure (Wang et al., 2014). The feature wavelengths including 2,122, 2,095, 2,169, and 2,041 nm in the range of 2,020 to 2,190 nm were attributed to the N—H and O—H stretching (Fernández-Ibañez et al., 2009). Moreover, more high-frequency wavelengths were observed at 1,612 nm, which had not been widely reported in previous studies.

3.5.4. Spatio-temporal distribution patterns and visualization of aflatoxin in peanut kernels

Fig. S6 showed the spatio-temporal distribution of AFB_1 and total aflatoxin in peanut kernels. The color gradient bar on the right showed that the AFB_1 content ranged from 0 to 130 μg/kg, and the total aflatoxin content ranged from 0 to 180 μg/kg. The IVISSA-SPA-PLSR model was used to predict the content of AFB_1 and total aflatoxin in each pixel. The value of content was then converted into a corresponding color using Python 3.8. Therefore, the color of each pixel was used to determine the spatio-temporal distribution of AFB_1 and total aflatoxin. Firstly, as shown in Fig. S6(a), the content of AFB_1 in peanut kernels increased continuously with the increase in contamination time. Then, AFB_1 penetrated from the seed coat to the cotyledon of the peanut kernels due to the contamination by *Aspergillus flavus*. In addition, the spatio-temporal distribution of total aflatoxin was similar to that of AFB_1, and the content of total aflatoxin was obviously higher than that of AFB_1 over time in Fig. S6(b). Overall, all results were consistent with the above analysis of the process of the peanut kernels contaminated by *Aspergillus flavus*.

4. Conclusion

Firstly, the analysis of spatio-temporal distribution patterns of aflatoxin indicated that the content of aflatoxin increased significantly on the 5th day and exceeded the safety limits, reaching a peak on the 9th day. AFB_1 remained the most important aflatoxin produced by *Aspergillus flavus* in peanut kernels. The contamination of *Aspergillus flavus* caused aflatoxin to penetrate from the seed coat to the cotyledon of the peanut kernels, resulting in an increase in aflatoxin content. Then, the spectral differences between the control groups and contaminated groups indicated that *Aspergillus flavus* contamination caused physical and chemical changes in the *Aspergillus flavus*-peanut kernels interaction. Moreover, although PCA results were effective in identifying contaminated peanut kernels, the supervised discriminant model accurate classified the control-contaminated group and the control-different contamination time groups, and distinguished the contamination time of contaminated peanut kernels, LDA achieved the best classification effect, with an accuracy rate of ≥98.10%, and the result showed a

Table 3
Parameter values of regression models performance.

Aflatoxins category	Modeling methods	Variable selection methods	R^2_C	RMSEC (μg/kg)	R^2_{CV}	RMSECV (μg/kg)	R^2_V	RMSEV (μg/kg)	RPD	LVs	Number of variables	LOD (μg/kg)	LOQ (μg/kg)	Slope	Interc-ept
Total aflatoxin	PLSR	None	0.8626	13.8836	0.6458	22.7451	0.8409	12.9280	2.5631	12	209	47.0262	141.0787	0.8746	4.1429
		SPA	0.5514	25.0856	0.4894	26.6245	0.8207	13.7240	2.4144	6	9	48.4680	145.4041	0.8110	2.3230
		RC	0.8122	16.2293	0.7014	20.7398	0.7944	14.6920	2.2553	14	15	55.3858	166.1574	0.8112	6.5909
		CARS	0.8347	15.2861	0.7539	18.7013	0.7931	14.7423	2.2477	9	14	57.3647	172.0941	0.7569	5.8469
		IVISSA	0.8795	13.0017	0.7646	18.5424	0.8320	13.2833	2.4945	12	81	50.1675	150.5025	0.7977	5.7962
		IVISSA-SPA	**0.5731**	**24.4711**	**0.4910**	**26.8576**	**0.8559**	**12.1493**	**2.7274**	**7**	**10**	**45.7429**	**137.2286**	**0.8033**	**6.0386**
	PCR	None	0.8515	14.4359	0.6669	21.8846	0.8340	13.5320	2.4487	21	209	65.7042	197.1127	0.8374	3.8561
		SPA	0.5754	24.4050	0.5058	25.4840	0.8207	13.7240	2.4144	9	9	48.4681	145.4044	0.8110	2.8323
		RC	0.8111	16.2755	0.6925	21.6214	0.8088	14.1692	2.3386	14	15	51.6818	155.0454	0.8389	7.5963
		CARS	0.8342	15.2535	0.7652	18.4500	0.7861	14.9889	2.2107	11	14	62.1674	186.5023	0.7192	8.0186
		IVISSA	0.8775	13.1121	0.7748	18.0758	0.8165	13.8831	2.3868	18	81	54.3217	162.9652	0.7770	7.2988
		IVISSA-SPA	0.5480	25.1806	0.4620	26.6740	0.8559	12.1494	2.7274	7	10	45.7427	137.2281	0.8033	6.0385
Aflatoxin B_1	PLSR	None	0.8701	9.0027	0.7086	13.8758	0.8493	9.0476	2.6342	11	209	31.3756	94.1268	0.8043	3.8937
		SPA	0.6625	14.5095	0.6376	15.8300	0.8638	8.6030	2.7703	6	8	30.1239	90.3716	0.8574	2.7569
		RC	0.8496	9.6816	0.7354	12.9143	0.5812	15.0836	1.5800	13	15	45.7446	137.2339	0.9858	−2.9243
		CARS	0.8818	8.5873	0.8113	10.9383	0.7780	10.9815	2.1703	11	21	36.2230	108.6691	0.8818	0.2602
		IVISSA	0.8854	8.4541	0.7497	12.7806	0.8608	8.6960	2.7407	12	92	30.3709	91.1128	0.8645	2.7616
		IVISSA-SPA	**0.6319**	**15.1547**	**0.6178**	**16.0908**	**0.8663**	**8.5242**	**2.7959**	**5**	**9**	**29.3722**	**88.1166**	**0.8474**	**2.2239**
	PCR	None	0.8687	9.0500	0.7063	13.2464	0.8527	8.9458	2.6641	20	209	31.9742	95.9226	0.8091	3.0669
		SPA	0.6660	14.4359	0.6322	15.3949	0.8640	8.5947	2.7730	7	8	30.1265	90.3796	0.8554	2.7710
		RC	0.8499	9.6778	0.7134	13.2362	0.6051	14.6467	1.6272	15	15	46.5968	139.7903	0.9407	−1.3346
		CARS	0.8801	8.6481	0.8213	10.6423	0.8407	9.3024	2.5620	11	21	28.6235	85.8705	0.9109	−0.9563
		IVISSA	0.8776	8.7373	0.7761	12.2088	0.8435	9.2216	2.5844	19	92	33.4353	100.3060	0.8189	3.4252
		IVISSA-SPA	0.6055	15.6889	0.5775	16.4255	0.8644	8.5820	2.7771	6	9	29.2134	87.6403	0.8620	1.8714
Aflatoxin B_2	PLSR	None	0.7180	6.1665	0.3967	9.0840	0.7150	5.1339	1.9153	10	209	26.2837	78.8510	0.7307	2.3634
		SPA	0.4829	8.3502	0.4372	8.6455	0.7390	4.9133	2.0013	6	11	22.4430	67.3291	0.6559	2.4239
		RC	0.6722	6.6478	0.4473	0.8861	0.7353	4.9475	1.9875	13	17	21.1507	63.4521	0.7195	2.8965
		CARS	**0.7218**	**6.1240**	**0.6019**	**7.4420**	**0.7864**	**4.4444**	**2.2124**	**8**	**26**	**21.2209**	**63.6628**	**0.6273**	**2.8402**
		IVISSA	0.7535	5.7644	0.5981	7.3502	0.7652	4.6601	2.1100	10	73	23.6015	70.8045	0.5952	3.2639
		IVISSA-SPA	0.4631	8.5085	0.4384	8.7921	0.7203	5.0859	1.9334	5	10	26.9548	80.8643	0.5717	3.5732
	PCR	None	0.6794	6.5746	0.4297	9.0965	0.7422	4.8828	2.0138	16	209	22.2890	66.8670	0.6490	2.3128
		SPA	0.4486	8.6219	0.4030	8.9466	0.7349	4.9515	1.9858	7	11	22.6100	67.8301	0.6562	2.4460
		RC	0.6724	6.6460	0.4498	8.7602	0.7516	4.7929	2.0516	16	17	21.1399	63.4196	0.6952	2.9757
		CARS	0.7221	6.1213	0.6311	7.2673	0.7278	5.0171	1.9599	10	26	28.0356	84.1069	0.5375	3.6964
		IVISSA	0.7453	5.8604	0.6246	7.2760	0.7201	5.0882	1.9325	13	73	25.9582	77.8745	0.5771	2.8826
		IVISSA-SPA	0.5030	8.1857	0.4060	8.9186	0.6871	5.3794	1.8279	9	10	32.1543	96.4630	0.5109	4.4790
Aflatoxin G_2	PLSR	None	0.6477	0.9835	0.3387	1.3698	0.5675	0.9859	1.5548	9	209	5.0307	15.0921	0.6125	0.7668
		SPA	**0.6561**	**0.9717**	**0.5568**	**1.2697**	**0.6612**	**0.8726**	**1.7567**	**10**	**22**	**4.0364**	**12.1092**	**0.6535**	**0.5799**
		RC	0.4142	1.2682	0.3303	1.3621	0.3830	1.1776	1.3017	3	10	11.0645	33.1934	0.3261	0.7841
		CARS	0.6866	0.9276	0.5502	1.1302	0.5065	1.0532	1.4554	9	16	6.7253	20.1760	0.4803	0.6318
		IVISSA	0.6549	0.9735	0.4868	1.1822	0.5856	0.9651	1.5883	7	56	5.0736	15.2208	0.5789	0.6454
		IVISSA-SPA	0.6641	0.9604	0.5655	1.2279	0.6412	0.8980	1.7070	9	25	3.7832	11.3495	0.7089	0.5676
	PCR	None	0.6300	1.0080	0.3879	1.3174	0.5722	0.9806	1.5632	15	209	5.6397	16.9191	0.5260	0.7527
		SPA	0.6992	0.9087	0.5405	1.2838	0.6450	0.8933	1.7160	20	22	4.5342	13.6026	0.6006	0.5967
		RC	0.4195	1.2620	0.3266	1.3715	0.3789	1.1815	1.2974	4	10	11.1593	33.4778	0.3246	0.8027
		CARS	0.6932	0.9179	0.5783	1.0809	0.5030	1.0568	1.4505	11	16	6.8550	20.5649	0.4729	0.6662
		IVISSA	0.6560	0.9719	0.5088	1.1713	0.5385	1.0185	1.5050	11	56	5.6144	16.8433	0.5503	0.7115
		IVISSA-SPA	0.6501	0.9802	0.5746	1.0945	0.5252	1.0330	1.4839	11	25	5.4297	16.2892	0.5763	0.6905

Note: PLSR, partial least squares regression; PCR, principal component regression; SPA, projection algorithm; RC, regression coefficient; CARS, competitive adaptive reweighted sampling; IVISSA, interval variable iterative space shrinkage approach; IVISSA-SPA, interval variable iterative space shrinkage approach-successive projection algorithm; R^2_C, coefficient of determination of calibration set; RMSEC, root mean square error of calibration set; R^2_V, coefficient of determination of validation set; RMSEV, root mean square error of validation set; RPD, ratio of performance to deviation; LVs, optimal number of principal components; LOD, limit of detection; LOQ, limit of quantification.

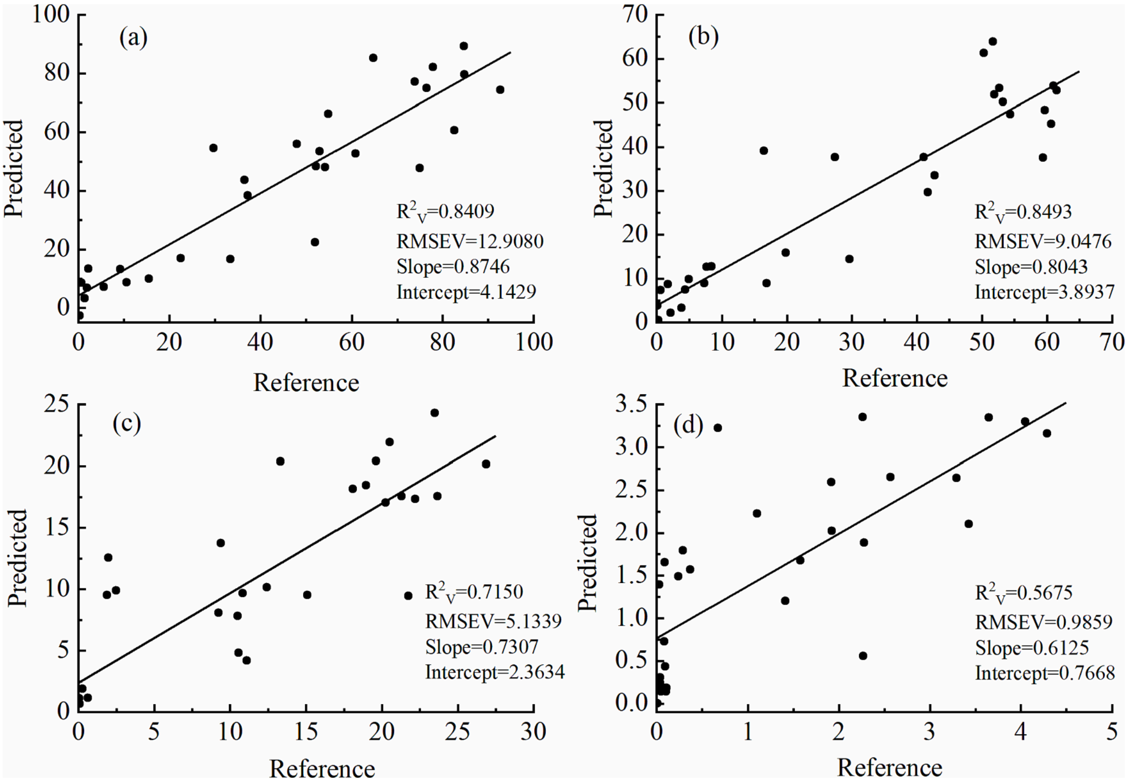

Fig. 3. Regression effect of PLSR in predicting aflatoxin content, (a) total aflatoxin, (b) AFB_1, (c) AFB_2, (d) AFG_2.

noticeable difference in the spectra between the control groups and contaminated groups. The supervised discriminant model accurately classified AFB_1 and total aflatoxin, with the average classification accuracy rate of AFB_1 being higher than that of total aflatoxin. Finally, the regression model's quantitative analysis revealed that IVISSA-SPA-PLSR could accurately predict the content of AFB_1 and total aflatoxin, with $R^2_V = 0.8663$, RMSEV = 8.5242 and RPD = 2.7959 for AFB_1 and $R^2_V = 0.8559$, RMSEV = 12.1493 and RPD = 2.7274 for total aflatoxin, respectively. Only general predictions could be made for the content of AFB_2, but the content of AFG_2 could not be effectively predicted. In addition, the selected characteristic wavelengths were associated with the changes in substance composition and cell structure of peanut kernel cells during contamination by *Aspergillus flavus*. This study offers a novelty method for quantitatively detecting aflatoxin and provides preparation for early aflatoxin warning.

CRediT authorship contribution statement

Zhen Guo: Investigation, Conceptualization, Methodology, Formal analysis, Writing – original draft. **Jing Zhang:** Software, Data curation, Validation, Writing – original draft. **Haowei Dong:** Investigation, Methodology, Formal analysis, Writing – review & editing. **Jiashuai Sun:** Investigation, Methodology, Supervision, Writing – review & editing. **Jingcheng Huang:** Methodology, Supervision, Resources, Writing – review & editing. **Shiling Li:** Project administration, Resources, Writing – review & editing. **Chengye Ma:** Supervision, Resources, Project administration, Writing – review & editing. **Yemin Guo:** Supervision, Resources, Software, Project administration, Funding acquisition, Writing – review & editing. **Xia Sun:** Supervision, Resources, Software, Project administration, Funding acquisition, Writing – review & editing.

Declaration of Competing Interest

The authors declare that they have no known competing financial interests or personal relationships that could have appeared to influence the work reported in this paper.

Data availability

Data will be made available on request.

Acknowledgments

This work was supported by the National Natural Science Foundation of China (No. 31772068), Shandong Provincial Science and Technology Achievement Transfer Subsidy (Lu-Yu Science and Technology Cooperation) (LYXZ10), Funding Project for the Central Government to Guide the Development of Local Science and Technology (YDZX2022163) and Shandong Province Major Applied Technology Innovation Project (SD2019NJ007).

Appendix A. Supplementary data

Supplementary data to this article can be found online at https://doi.org/10.1016/j.foodchem.2023.136441.

References

Achar, P. N., Hermetz, K., Rao, S., Apkarian, R., & Taylor, J. (2009). Microscopic studies on the *Aspergillus flavus* infected kernels of commercial peanuts in Georgia. *Ecotoxicology and Environmental Safety, 72*(8), 2115–2120. https://doi.org/10.1016/j.ecoenv.2009.04.002

Adedipe, O. E., Johanningsmeier, S. D., den Truong, V., & Yencho, G. C. (2016). Development and validation of a near-infrared spectroscopy method for the prediction of acrylamide content in french-fried potato. *Journal of Agricultural and Food Chemistry, 64*(8), 1850–1860. https://doi.org/10.1021/acs.jafc.5b04733

Bankole, S. A., Ogunsanwo, B. M., & Eseigbe, D. A. (2005). Aflatoxins in Nigerian dry-roasted groundnuts. *Food Chemistry, 89*(4), 503–506. https://doi.org/10.1016/j.foodchem.2004.03.004

Berardo, N., Pisacane, V., Battilani, P., Scandolara, A., Pietri, A., & Marocco, A. (2005). Rapid detection of kernel rots and mycotoxins in maize by near-infrared reflectance spectroscopy. *Journal of Agricultural and Food Chemistry, 53*(21), 8128–8134. https://doi.org/10.1021/jf0512297

Campos, W. E. O., Rosas, L. B., Neto, A. P., Mello, R. A., & Vasconcelos, A. A. (2017). Extended validation of a sensitive and robust method for simultaneous quantification of aflatoxins B_1, B_2, G_1 and G_2 in Brazil nuts by HPLC-FLD. *Journal of Food Composition and Analysis, 60*, 90–96. https://doi.org/10.1016/j.jfca.2017.03.014

Chu, X., Wang, W., Yoon, S. C., Ni, X., & Heitschmidt, G. W. (2017). Detection of aflatoxin B_1 (AFB_1) in individual maize kernels using short wave infrared (SWIR) hyperspectral imaging. *Biosystems Engineering, 157*, 13–23. https://doi.org/10.1016/j.biosystemseng.2017.02.005

Ding, X., Li, P., Bai, Y., & Zhou, H. (2012). Aflatoxin B_1 in post-harvest peanuts and dietary risk in China. *Food Control, 23*(1), 143–148. https://doi.org/10.1016/j.foodcont.2011.06.026

Fernández-Ibañez, V., Soldado, A., Martínez-Fernández, A., & de la Roza-Delgado, B. (2009). Application of near infrared spectroscopy for rapid detection of aflatoxin B_1 in maize and barley as analytical quality assessment. *Food Chemistry, 113*(2), 629–634. https://doi.org/10.1016/j.foodchem.2008.07.049

Food and Agriculture Organization (FAO) (2004). Worldwide regulations for mycotoxins in food and feed in 2003. FAO Food and Nutrition, 81.

Freitag, S., Sulyok, M., Logan, N., Elliott, C. T., & Krska, R. (2022). The potential and applicability of infrared spectroscopic methods for the rapid screening and routine analysis of mycotoxins in food crops. *Comprehensive Reviews in Food Science and Food Safety, 21*(6), 5199–5224. https://doi.org/10.1111/1541-4337.13054

Gao, J., Zhao, L., Li, J., Deng, L., Ni, J., & Han, Z. (2021). Aflatoxin rapid detection based on hyperspectral with 1D-convolution neural network in the pixel level. *Food Chemistry, 360*, Article 129968. https://doi.org/10.1016/j.foodchem.2021.129968

Ghali, R., Belouaer, I., Hdiri, S., Ghorbel, H., Maaroufi, K., & Hedilli, A. (2009). Simultaneous HPLC determination of aflatoxins B_1, B_2, G_1 and G_2 in Tunisian sorghum and pistachios. *Journal of Food Composition and Analysis, 22*(7–8), 751–755. https://doi.org/10.1016/j.jfca.2009.04.009

He, X., Yan, C., Jiang, X., Shen, F., You, J., & Fang, Y. (2021). Classification of aflatoxin B_1 naturally contaminated peanut using visible and near-infrared hyperspectral imaging by integrating spectral and texture features. *Infrared Physics and Technology, 114*, Article 103652. https://doi.org/10.1016/j.infrared.2021.103652

Higgs, J. (2003). The beneficial role of peanuts in the diet–Part 2. *Nutrition & Food Science, 33*(2), 56–64. https://doi.org/10.1108/00346650310466637

Huang, C., Li, X., & Wen, Y. (2021). AN OTSU image segmentation based on fruitfly optimization algorithm. *Alexandria Engineering Journal, 60*(1), 183–188. https://doi.org/10.1016/j.aej.2020.06.054

Jiang, J., Qiao, X., & He, R. (2016). Use of Near-Infrared hyperspectral images to identify moldy peanuts. *Journal of Food Engineering, 169*, 284–290. https://doi.org/10.1016/j.jfoodeng.2015.09.013

Kaya-Celiker, H., Mallikarjunan, P. K., & Kaaya, A. (2015). Mid-infrared spectroscopy for discrimination and classification of Aspergillus spp. contamination in peanuts. *Food Control, 52*, 103–111. https://doi.org/10.1016/j.foodcont.2014.12.013

Kimuli, D., Wang, W., Wang, W., Jiang, H., Zhao, X., & Chu, X. (2018). Application of SWIR hyperspectral imaging and chemometrics for identification of aflatoxin B_1 contaminated maize kernels. *Infrared Physics and Technology, 89*, 351–362. https://doi.org/10.1016/j.infrared.2018.01.026

Krska, R., Leslie, J. F., Haughey, S., Dean, M., Bless, Y., McNerney, O., … Elliott, C. (2022). Effective approaches for early identification and proactive mitigation of aflatoxins in peanuts: An EU–China perspective. *Comprehensive Reviews in Food Science and Food Safety, 21*(4), 3227–3243. https://doi.org/10.1111/1541-4337.12973

Liu, R., Chang, M., Jin, Q., Huang, J., Liu, Y., & Wang, X. (2011). Degradation of aflatoxin B_1 in aqueous medium through UV irradiation. *European Food Research and Technology, 233*(6), 1007–1012. https://doi.org/10.1007/s00217-011-1591-9

Liu, Z., Jiang, J., Qiao, X., Qi, X., Pan, Y., & Pan, X. (2020). Using convolution neural network and hyperspectral image to identify moldy peanut kernels. *LWT, 132*, Article 109815. https://doi.org/10.1016/j.lwt.2020.109815

Long, Y., Huang, W., Wang, Q., Fan, S., & Tian, X. (2022). Integration of textural and spectral features of Raman hyperspectral imaging for quantitative determination of a single maize kernel mildew coupled with chemometrics. *Food Chemistry, 372*, Article 131246. https://doi.org/10.1016/j.foodchem.2021.131246

Lu, Y., Jia, B., Yoon, S. C., Zhuang, H., Ni, X., Guo, B., … Wang, W. (2022). Spatio-temporal patterns of *Aspergillus flavus* infection and aflatoxin B_1 biosynthesis on maize kernels probed by SWIR hyperspectral imaging and synchrotron FTIR microspectroscopy. *Food Chemistry, 382*, Article 132340. https://doi.org/10.1016/j.foodchem.2022.132340

Mishra, G., Panda, B. K., Ramirez, W. A., Jung, H., Singh, C. B., Lee, S. H., & Lee, I. (2022). Application of SWIR hyperspectral imaging coupled with chemometrics for rapid and non-destructive prediction of Aflatoxin B_1 in single kernel almonds. *LWT, 155*, Article 112954. https://doi.org/10.1016/j.lwt.2021.112954

Mphande, F. A., Siame, B. A., & Taylor, J. E. (2004). Fungi, aflatoxins, and cyclopiazonic acid associated with peanut retailing in Botswana. *Journal of Food Protection, 67*(1), 96–102. https://doi.org/10.4315/0362-028x-67.1.96

Qiao, X., Jiang, J., Qi, X., Guo, H., & Yuan, D. (2017). Utilization of spectral-spatial characteristics in shortwave infrared hyperspectral images to classify and identify fungi-contaminated peanuts. *Food Chemistry, 220*, 393–399. https://doi.org/10.1016/j.foodchem.2016.09.119

Sharma, S., Choudhary, B., Yadav, S., Mishra, A., Mishra, V. K., Chand, R., … Pandey, S. P. (2021). Metabolite profiling identified pipecolic acid as an important component of peanut seed resistance against *Aspergillus flavus* infection. *Journal of Hazardous Materials, 404*, Article 124155. https://doi.org/10.1016/j.jhazmat.2020.124155

Shen, F., Wu, Q., Liu, P., Jiang, X., Fang, Y., & Cao, C. (2018). Detection of Aspergillus spp. contamination levels in peanuts by near infrared spectroscopy and electronic nose. *Food Control, 93*, 1–8. https://doi.org/10.1016/j.foodcont.2018.05.039

Stuart, B. (2004). *Infrared spectroscopy: Fundamentals and Applications* (p. 86). John Wiley & Sons.

Sun, J., Shi, X., Zhang, H., Xia, L., Guo, Y., & Sun, X. (2019). Detection of moisture content in peanut kernels using hyperspectral imaging technology coupled with chemometrics. *Journal of Food Process Engineering, 42*(7), 13263. https://doi.org/10.1111/jfpe.13263

Sun, Y., Yuan, M., Liu, X., Su, M., Wang, L., Zeng, Y., … Nie, L. (2021). A sample selection method specific to unknown test samples for calibration and validation sets based on spectra similarity. *Spectrochimica Acta-Part A: Molecular and Biomolecular Spectroscopy, 258*, Article 119870. https://doi.org/10.1016/j.saa.2021.119870

Tao, F., Yao, H., Hruska, Z., Rajasekaran, K., Qin, J., & Kim, M. (2021). Use of line-scan Raman hyperspectral imaging to identify corn kernels infected with *Aspergillus flavus*. *Journal of Cereal Science, 102*, Article 103364. https://doi.org/10.1016/j.jcs.2021.103364

Wang, Q., Wu, G., Pian, F., Shan, P., Li, Z., & Ma, Z. (2021). Simultaneous detection of glucose, triglycerides, and total cholesterol in whole blood by Fourier-Transform Raman spectroscopy. *Spectrochimica Acta-Part A: Molecular and Biomolecular Spectroscopy, 260*, Article 119906. https://doi.org/10.1016/j.saa.2021.119906

Wang, W., Heitschmidt, G. W., Ni, X., Windham, W. R., Hawkins, S., & Chu, X. (2014). Identification of aflatoxin B_1 on maize kernel surfaces using hyperspectral imaging. *Food Control, 42*, 78–86. https://doi.org/10.1016/j.foodcont.2014.01.038

Wold, S., Sjöström, M., & Eriksson, L. (2001). PLS-regression: A basic tool of chemometrics. *Chemometrics and Intelligent Laboratory Systems, 58*(2), 109–130. https://doi.org/10.1016/S0169-7439(01)00155-1

Wu, Q., & Xu, H. (2020). Design and development of an on-line fluorescence spectroscopy system for detection of aflatoxin in pistachio nuts. *Postharvest Biology and Technology, 159*, Article 111016. https://doi.org/10.1016/j.postharvbio.2019.111016

Wu, Q., Xie, L., & Xu, H. (2018). Determination of toxigenic fungi and aflatoxins in nuts and dried fruits using imaging and spectroscopic techniques. *Food Chemistry, 252*, 228–242. https://doi.org/10.1016/j.foodchem.2018.01.076

Yin, J., Xia, Y., & Lu, M. (2012). Concentration profiles of collagen and proteoglycan in articular cartilage by Fourier transform infrared imaging and principal component regression. *Spectrochimica Acta-Part A: Molecular and Biomolecular Spectroscopy, 88*, 90–96. https://doi.org/10.1016/j.saa.2011.12.002

Yuan, D., Jiang, J., Qi, X., Xie, Z., & Zhang, G. (2020). Selecting key wavelengths of hyperspectral imagine for nondestructive classification of moldy peanuts using ensemble classifier. *Infrared Physics and Technology, 111*, 13058. https://doi.org/10.1016/j.infrared.2020.103518